International Journal of Biological Macromolecules 227 (2023) 590–600

Contents lists available at ScienceDirect

International Journal of Biological Macromolecules

journal homepage: www.elsevier.com/locate/ijbiomac

Inhibitory effects of fluorinated benzenesulfonamides on insulin fibrillation

Saeid Hadi Ali Janvand [a,b], Lucy Kate Ladefoged [c], Asta Zubrienė [d], Andrius Sakalauskas [d], Gunna Christiansen [e], Virginija Dudutienė [d], Birgit Schiøtt [c], Daumantas Matulis [d], Vytautas Smirnovas [d], Daniel E. Otzen [a,*]

[a] Interdisciplinary Nanoscience Center (iNANO), Aarhus University, Gustav Wieds Vej 14, 8000 Aarhus C, Denmark
[b] Institute of Biochemistry and Biophysics (IBB), University of Tehran, Tehran, Iran
[c] iNANO and Department of Chemistry, Aarhus University, 8000 Aarhus C, Denmark
[d] Department of Biothermodynamics and Drug Design, Institute of Biotechnology, Life Sciences Center, Vilnius University, Vilnius, Lithuania
[e] Department of Health Science and Technology, Medical Microbiology and Immunology, Aalborg University, Fredrik Bajers Vej 3b, DK-9220 Aalborg Ø, Denmark

ARTICLE INFO

Keywords:
Insulin
Protein fibrillation inhibitors
Carbonic anhydrase inhibitors
Sulfonamide compounds

ABSTRACT

Amyloid fibrils are protein aggregates formed by protein assembly through cross β structures. Inhibition of amyloid fibril formation may contribute to therapy against amyloid-related disorders like Parkinson's, Alzheimer's, and type 2 diabetes. Here we report that several fluorinated sulfonamide compounds, previously shown to inhibit human carbonic anhydrase, also inhibit the fibrillation of different proteins. Using a range of spectroscopic, microscopic and chromatographic techniques, we found that the two fluorinated sulfonamide compounds completely inhibit insulin fibrillation over a period of 16 h and moderately suppress α-synuclein and Aβ fibrillation. In addition, these compounds decreased cell toxicity of insulin incubated under fibrillation-inducing conditions. We ascribe these effects to their ability to maintain insulin in the native monomeric state. Molecular dynamic simulations suggest that these compounds inhibit insulin self-association by interacting with residues at the dimer interface. This highlights the general anti-aggregative properties of aromatic sulfonamides and suggests that sulfonamide compounds which inhibit carbonic anhydrase activity may have potential as therapeutic agents against amyloid-related disorders.

1. Introduction

Many proteins lose their native structure and form amyloid-like fibrils under denaturing conditions [1–4] which partially unfold proteins to states with a high tendency to form aggregates [5] through exposure of hydrophobic groups and backbone amide groups [6]. Protein fibrillation or amyloid formation is associated with diseases such as spongiform encephalopathy, Huntington's diseases, prolactinomas, cardiac arrhythmias, atherosclerosis, rheumatoid arthritis, type 2 diabetes, Parkinson's and Alzheimer's disease (AD) [6–12]. Despite the lack of similarity between the sequences and structures of the proteins causing these diseases, their amyloid state share features such as cross β-sheet structures, the ability to bind fluorescent dyes such as thioflavin T (ThT) and the formation of threadlike and unbranched structures a few nanometers in diameter [13,14]. Oligomeric species, typically formed at early stages of aggregation, can bind to cell membranes and perturb their integrity, leading to cell death [15]. This has motivated many efforts to inhibit or modulate protein fibrillation and early stage aggregates by the use of *e.g.* chaperones [16], natural compounds [17], nanoparticles [18], peptides [19], small molecules [20,21], and polymers [22].

The aggregating species observed in these different diseases are formed in many different ways. In this study we focused on the inhibition of insulin fibrillation as a model for the fibrillation of globular protein by some new type of inhibitors. Insulin is a 51-residue hormone comprised of two peptide chains (A and B chain) connected by two

Abbreviations: AD, Alzheimer's disease; CA, carbonic anhydrase; ThT, thioflavin T; Aβ, amyloid beta peptide; α-Syn, alpha synuclein; APP, amyloid precursor protein; MDSIs, multiple daily subcutaneous injections; CSII, continuous subcutaneous insulin infusions; FBS, fetal bovine serum; DMEM, Dulbecco's Modified Eagle Medium; LDH, lactate dehydrogenase; AFM, atomic force microscopy; ATR-FTIR, attenuated total reflectance Fourier transform infrared spectroscopy; SEC, size exclusion chromatography; TEM, transmission electron microscopy; CD, circular dichroism; MD, molecular dynamics; RMSD, root mean squared deviation; RMSF, root mean squared fluctuation; MTT, 3-[4,5-dimethylthiazol-2-yl]-2,5 diphenyltetrazolium bromide.

* Corresponding author.
E-mail address: dao@inano.au.dk (D.E. Otzen).

https://doi.org/10.1016/j.ijbiomac.2022.12.105
Received 6 August 2022; Received in revised form 15 November 2022; Accepted 10 December 2022
Available online 15 December 2022

disulfide bonds [27]. Chain A consists of two helices (A2–A8 and A13–A19), while chain B has a single helix (B9–B19). Insulin is produced in β cells of pancreatic islets and regulates the sugar level in the bloodstream [28]. Insulin formulations are used in type I diabetes, either as multiple daily subcutaneous injections (MDSIs) or as continuous subcutaneous insulin infusions (CSII) [29]. Repeated subcutaneous injection of insulin can lead to the formation of amyloid deposits at the site of injection [30], preventing the absorption of insulin and control of blood glucose homeostasis [31]. Insulin aggregation requires unfolding, *i.e.* loss of native structure. Thus compounds which bind and stabilize insulin's native state should reduce insulin aggregation by simple mass-action effects. Indeed we have previously shown that compounds such as derivatives of the opium poppy compound noscapine can bind specifically to insulin in the native monomeric state and prevent its aggregation [32]. Also, patients with Parkinson's disease develop an autoimmune response against the insulin oligomers and fibrils, suggesting a role for these structures during the onset of Parkinson's disease [33].

To check whether these new type of compounds might generally suppress protein aggregation we tested the effects of them on α-synuclein (α-Syn) and amyloid beta peptide (Aβ) as two intrinsically disordered proteins. Aβ is produced from amyloid precursor protein (APP) by proteolytic activity of β- and γ secretase activity in the brain. Aβ accumulation and formation of plaques in the brain contribute critically to the initiation and propagation of AD. Current AD therapeutic strategies to stop or reverse the progression of AD include attempts to inhibit Aβ fibril formation, remodel the amyloid aggregates, or degrade the insoluble fibrils [23]. The synucleinopathies are neurodegenerative diseases characterized by the accumulation of aggregates mainly composed of the protein α-synuclein in different regions of the brain [6]. Many different approaches are currently attempting to reduce α-Syn oligomer formation or fibrillation through the use of *e.g.* small molecules, immunotherapy or gene silencing [24]. In contrast, insulin aggregates formed in *e.g.* type 2 diabetes are formed by what is normally a natively folded protein [25,26].

We recently identified a new class of small molecules as inhibitors of α-Syn fibril formation, namely compounds with a common (4-hydroxynaphthalen-1-yl)sulfonamide core [34], which maintain high amounts of soluble α-Syn throughout the fibrillation process. Interestingly, sulfonamides also inhibit the activity of carbonic anhydrase (CA). This enzyme catalyzes the reversible hydration of carbon dioxide to bicarbonate anion and a proton, a critical process in physiological pH regulation [35]. CA is involved in many diseases like glaucoma, cancer, and epilepsy [36–38], and the most prevalent approach to the design of CA inhibitor is the ring and tail approach [39], in which the aromatic group (the ring) increases binding capability while the flexible fragment (the tail) improves aqueous solubility. This has led to the development of inhibitors such as benzenesulfonamides [40]. The sulfonamide group acts as an "anchor" in the active site of CA, while the substituents on the benzene ring strongly affect the binding affinity and selectivity for particular CA isozymes. A particularly strong class of CA inhibitors are benzenesulfonamides which contain halogen atoms, typically fluorine which is a powerful electron-withdrawing substituent [41]. Fluorinated compounds were also found to inhibit fibrillation of α-Syn [32,33]. Inspired by these observations, we tried to test the effects of this novel type of CA activity inhibitors that contained both sulfonamide and fluorine group against insulin, α-Syn and Aβ. We show that some CA inhibitors have strong inhibitory effects on insulin, α-Syn and Aβ fibrillation. We attribute the strong effect on insulin fibrillation to an ability to bind specifically to the folded monomeric state and prevent its self-assembly. The more modest effect on the other proteins may reflect a general but rather weak ability to suppress growth of aggregates. Our work introduces a multipurpose inhibitor that not only inhibits CAs, but also slows down or prevents aggregation of several different proteins.

2. Materials and methods

2.1. Materials

Fetal bovine serum (FBS), penicillin-streptomycin, and Dulbecco's Modified Eagle Medium (DMEM) were from Gibco BRL (Gaithersburg, MD). The lactate dehydrogenase (LDH) measurement kit was from Thermo Scientific (Roskilde, DK). Expression and purification of α-Syn were carried out as described in [41]. Aβ(1-40) was from Chinese Peptide (Hangzhou Economic and Technological Development Zone, China). Human insulin (91077C) and all other chemicals were purchased from Sigma Aldrich (St. Louis, MO). PBS solutions contained 50 mM NaHPO4, pH 7.4, 150 mM NaCl and 2.5 mM EDTA.

2.2. Preparation of inhibitors

The compounds investigated in this study were synthesized as described in [42,43]. All compounds were dissolved in DMSO to a final concentration of 10 to 50 mM, and diluted to 5 to 200 μM as required.

2.3. Kinetics of insulin fibrillation

ThT was employed to follow the kinetics of protein fibrillation by using excitation and emission wavelength of 445 and 485 nm respectively.

2.3.1. Insulin

0.5 mg human insulin was dissolved in 60 μL of 20 mM HCl pH 1.6 containing 150 mM NaCl, then by adding 940 μL of PBS, the pH was raised to 7.2, giving 85 μM final insulin concentration (final concentration calculated using an extinction coefficient of 1400 M^{-1} cm^{-1} at 276 nm). 150 μL of samples in a 96 well plate (Nunc, Thermo Fischer Scientific, Roskilde, Denmark) were sealed with clear tape with one 3-mm glass bead (Merck) per well with 40 μM ThT final concentration and 5–200 μM sulfonamide compound (from stocks of 50 mM in DMSO; final DMSO concentration in all cases <1 %). Plates were monitored on a Genios Pro fluorescence plate reader (Tecan, Männedorf, Switzerland) at 37 °C with 300 rpm orbital shaking between each 5 min cycle. The lag time was estimated as the linearly extrapolated x-axis intercept of the growth phase.

2.3.2. Aβ(1-40)

Aβ(1-40) was dissolved in DMSO to 6 mM, then diluted with PBS to 50 μM and fibrillation was monitored by incubating samples in the presence of a different concentration of inhibitors at 37 °C without shaking.

2.3.3. α-Syn

The protein was incubated in PBS 70 μM in the presence of different compounds with one 3-mm glass bead in each well and 300 rpm between the readings for 12 min at 37 °C.

2.4. Circular dichroism (CD)

Far-UV CD spectra were recorded for insulin monomer and fibrillated samples on a Chirascan CD spectrophotometer (Applied Photophysics, Surrey, UK) in a 1 mm quartz crystal cuvette with 0.3 nm step size and 0.5 nm bandwidth from 260 to 200 nm using three measurement repeats. Fibrillated samples were collected at different times of incubation, sonicated for 10 min in a Sonorex Digitec ultrasonic bath (Bandelin, Berlin, Germany) and diluted to 15 μM in PBS. Buffer spectra were subtracted from each sample.

2.5. Attenuated Total Reflectance Fourier Transform Infrared Spectroscopy (ATR-FTIR)

To determine the spectrum of insulin fibrils, samples from different time points were centrifuged (13,000 rpm for 15 min), and the pellet suspend in PBS. 2 μL of the sample was spread on the crystal surface and dried under nitrogen gas. Spectra were recorded using a Tensor 27 FTIR spectrophotometer (Bruker, Billerica, Massachusetts, USA) with 68 scans. The sample chamber was continuously purged with nitrogen. Atmospheric compensation, baseline correction, and second-derivative spectra of curves were carried out with OPUS software version 5.5.

2.6. Size exclusion chromatography (SEC)

To determine the amount of monomer remaining in the samples collected at different time points of fibrillation, samples were spun (13,500 rpm for 10 min) before running on a 24 mL Superose 6 10/300 column (GE Healthcare). 250 μL of supernatant was loaded on the column at a flow rate of 0.5 mL/min using an Äkta Pure protein purification system (GE Healthcare) and absorbance was recorded at 280 nm.

2.7. Transmission electron microscopy (TEM)

The morphology of insulin fibrils in the absence and presence of inhibitors was determined using TEM. 5 μL of sample was transferred to a 400-mesh carbon-coated glow-discharged Ni grid for 30 s. After washing the grid using 2 drops of double-distilled water, samples were stained with 1 % (w/v) phosphotungstic acid (pH 6.8) and blotted dry on a filter paper. Electron microscopy was done on a JEOL 1010 transmission electron microscope (JEM 1010, Tokyo, Japan) operated at 60 keV. Images were recorded using an electron-sensitive CCD camera (KeenView, Olympus, Tokyo, Japan).

2.8. Atomic force microscopy (AFM)

The samples for AFM images were collected after kinetic measurements and scanned similarly as previously described [44]. In short, 40 μL of freshly prepared 0.5 % (v/v) APTES (Sigma-Aldrich, cat. No. 440140) in MilliQ water was deposited on freshly cleaved mica and incubated for 5 min. Then, the mica was rinsed with 2 mL of MilliQ water and dried under a gentle airflow. 30 μL of each sample was deposited on the functionalized surface and incubated for another 5 min. Prepared samples were rinsed with 2 mL of MilliQ water and dried under a gentle airflow. AFM imaging was performed using a Dimension Icon (Bruker) atomic force microscope.1024 × 1024 pixel resolution images were analysed using Gwyddion 2.5.5 software.

2.9. MTT reduction assay

This cell viability assay was performed on human neuroblastoma cells (SH-SY5Y) to measure the reduction of MTT (3-[4,5-dimethylthiazol-2-yl]-2,5 diphenyltetrazolium bromide) to insoluble formazan by mitochondrial succinate dehydrogenase. Cells were cultured in DMEM supplemented with 10 % FBS, 100 units/mL penicillin, and 100 μg/mL streptomycin to a density of 6×10^4 cell/mL in 96 well plates under at 37 °C and 5 % CO_2 in an incubator. After 24 h the medium was replaced with a fresh media containing 0 μM or 200 μM of inhibitors only, insulin fibrils only (formed as described in Section 2.2 by incubation at 37 °C for 2, 4, 6, 8, 9 and 12 h) or insulin samples incubated in the presence of 200 μM inhibitors under the same conditions as insulin alone. After 1 day of incubation with samples, cells were washed with PBS, the supernatant was removed and fresh media containing 10 % MTT (5 mg/mL) in PBS was added to each well. Then samples were further incubated for 4 h at 37 °C. The medium was aspirated from each well and 100 μL of DMSO was added per well to solubilize formazan formed by shaking for 1 h at room temperature. Subsequently, the absorbance was recorded at 570 nm on a Varioscan plate reader. The experiments were performed in triplicate and cell viability was calculated using the following equation:

$$\text{Cell viability } (\%) = 100 \times \text{Abs}_{570}{}^{\text{Treated cells}} / \text{Abs}_{570}{}^{\text{Control cells}}.$$

2.10. Lactate dehydrogenase (LDH) release assay

The release of LDH by membrane damage or lysis into culture media as an assay for measuring cell death, was performed on SH-SY5Y cells using an LDH assay kit (Thermo Scientific). In this assay, the extent of LDH released to media is quantified by measuring the oxidation of lactate to pyruvate mediated by LDH and simultaneously converting a tetrazolium dye to a red formazan derivative. Insulin-fibrillated samples taken from different times of fibrillation in the presence and absence of inhibitors were added to SH-SY5Y cells (40,000 cell/mL) and incubated for 1 day at 37 °C and 5 % CO_2 in an incubator. Thereafter, 100 μL growth medium was collected and the LDH activity was determined by measuring the absorbance at 490 nm and 690 nm according to the protocol provided by the kit. The total cellular LDH activity was determined by treating the cells with 0.1 % Triton. The percentage release of LDH from treated samples divided by the percentage release of LDH from untreated cells was used to determine LDH values.

2.11. Molecular dynamics (MD) simulations

The insulin structure was prepared as described [39] based on PDB entry 1TRZ [45], and had all termini charged, all amino acids in their default states at neutral pH, and all cysteines involved in disulfide bridges. The structure of each ligand (VR16-09, VR16-10, VD18-03, and VD12-34) was manually built in Maestro (Schrödinger Suite 2019, Schrödinger LLC, New York, NY) before being minimized and submitted to a conformational search using MacroModel available within Maestro. The lowest energy structure of each ligand was used as a starting point in system building as described below, but also for the parametrization process. Parameters for each ligand were obtained from the CHARMM-compatible CGenFF force field [37], *via* the paramchem webserver [47,48]. When no parameters were found, alternative parameters were selected based on analogy between functional groups and a penalty was reported. The associated penalties of each ligand were all low and no parameter validation was therefore performed. The molecular system was constructed by randomly orienting each ligand and then placing it near insulin at random using an in-house python script. This process was repeated ten times for each ligand resulting in ten separate molecular systems each containing one ligand and one insulin protein. Each molecular system was then solvated and ionized with NaCl to a concentration of 0.15 M mimicking the experimental conditions. The resulting systems were approximately $7 \times 7 \times 7$ nm^3. Each system was minimized and equilibrated individually before production runs according to the protocol outlined in Table 1.

All simulations were performed in Gromacs 2019.4 [49] using the CHARMM36m force field [50], the TIPS3P water model [51], and CHARMM-compatible ligand parameters from the CGenFF force field [46–48,52,53]. The vdW interactions were treated by cut-offs at 12 Å

Table 1
Simulation protocol.

Chronological step	Equilibration runs		Production run
	1	2	3
Ensemble	NVT	NPT	NPT
Duration	0.5 ns	1 ns	100 ns
Timestep	2 fs	2 fs	2 fs
Position restraints	Protein + ligand	Protein + ligand	None
Thermostat	Velocity rescale	Nose-Hoover	Nose-Hoover
Barostat	–	Parrinello-Rahman	Parrinello-Rahman

and a force-switch modifier after 10 Å, while electrostatic interactions were treated using PME. The neighbor list was maintained using Verlet buffer lists, and bonds linking hydrogen atoms to heavy atoms were restrained using LINCS [54]. The temperature was maintained at 310 K using a coupling time constant of 1, and pressure was maintained at 1 bar using a coupling time constant of 4, a compressibility factor of 4.5×10^{-5} and isotropic coupling to x, y and z dimensions.

3. Results

3.1. Comparison of the capability of sulfonamide compounds to inhibit protein fibrillation

The structures of compounds investigated in this study are shown in Fig. 1. The fibrillation of different proteins was monitored using the dye ThT, whose fluorescence emission at 485 nm is increased upon binding to fibrils. In the first step, we quantified the effects of 11 different compounds on α-Syn and Aβ fibril formation (Fig. 2). ThT time curves showed VR16-09 and VR16-10 to be the most potent inhibitors of α-Syn fibril formation in terms of overall ThT fluorescence (Fig. 2a), though only VR16-09 increased the lag time of fibrillation; the effect of both compounds on the ThT time profile saturated around 50 μM (Supplementary Fig. S1A). VR16-09 and VR16-10 also emerged as the best inhibitors of Aβ fibril formation (Fig. 2B and S1B) and affected both lag time and ThT intensity. The aggregation of Aβ was slowed down to such an extent that it did not reach a plateau during the incubation period (Fig. S1B).

To check the generality of the compounds' inhibitory activity, we also tested them on insulin fibrillation. ThT fluorescence during insulin fibrillation followed a sigmoidal curve with a lag phase, a growth phase, and a plateau (Fig. 3), providing information about the lag time, rate of fibril formation, and the maximum level of ThT intensity during fibrillation, respectively. Four compounds (VR16-09, VR16-10, VD12-09, and VD11-4-2) completely suppressed ThT fluorescence at 200 μM while several others either increased or decreased the lag phase; a few had no effect (Fig. 3A, summarized in Fig. 3B, C). Subsequent dose dependency studies of these four compounds showed that VR16-09 and VR16-10 completely suppressed ThT fluorescence already at 20 μM (Fig. 3D, Fig. S2), while VD11-4-2 and VD12-09 required higher concentrations. Given that insulin was the most promising candidate for aggregation inhibition by our compounds, we limited the remainder of the study to the effects of VR16-09, VR16-10, VD12-09, and VD11-4-2 on insulin fibrillation.

3.2. VR16-09 and VR16-10 maintain insulin in the native state

The ThT assay is an indirect assay for aggregation as its fluorescence can also be sensitive to other effects such as the displacement of ThT from the fibril binding sites by competing compounds [55]. We therefore turned to alternative techniques which could provide a more direct read-out of the structure and size of insulin species after incubation alone and with our benzenesulfonamides. Insulin samples aggregated alone and in the presence of different compounds were collected at the end of the incubation period and their secondary structure was investigated with CD and FTIR. In the presence of VR16-09 and VR16-10, insulin largely maintained its native secondary structure as seen by the far UV CD peaks at 208 and 222 nm, characteristic of insulin's native α-helix structure (Fig. 4A). This was confirmed by FTIR spectra which showed a single peak around 1658 cm^{-1} characteristic of α-helices (Fig. 4B). Furthermore, the presence of VR16-09 and VR16-10 retains a very significant amount of insulin in the monomeric state (compared to the complete loss of monomer in the absence of compounds) according to gel filtration chromatography (Fig. 4C with insert). In contrast, VD11-4-2 and VD12-09 led to a change in the secondary structure (CD minimum around 225 nm and FTIR peaks around 1630 cm^{-1}); however, the monomer population was still high according to SEC, indicating that the compounds maintained insulin in a non-native but monomeric state, which was also consistent with the lack of ThT signal.

For more insight, samples were collected at different time points of the fibrillation process. In the control sample, without the presence of any compound, insulin starts to decrease in α-helix content at the beginning of the elongation phase and loses its structure completely at the end of the fibrillation process (Fig. S3A). Similarly, coincubation of insulin with VD11-4-2 leads to a reduction of α-helix content from the beginning of the elongation phase shown in CD spectra, in accordance with its related FTIR spectra with disappearing of α-helix and emerging of an intense peak around 1630–1640 cm^{-1}, attributed to the formation of parallel β sheets (Fig. S3B). VD12-09 is better able to maintain insulin in the native state than VD11-4-2. CD and FTIR spectra recorded at different times of fibrillation showed that incubation of insulin with VD12-09 preserved the native state of protein right up to the beginning of the plateau phase, after which the α-helical and β-sheet content of protein decreased and increased, respectively. In contrast to VD11-4-2 and VD12-09, the compounds of VR16-09 and VR16-10 maintained the native state of insulin during incubation. VR16-10 led to a minor structural rearrangement due to a small extent of fibrillation (as shown in FTIR spectra Fig. S3B); however, the native structure of insulin was

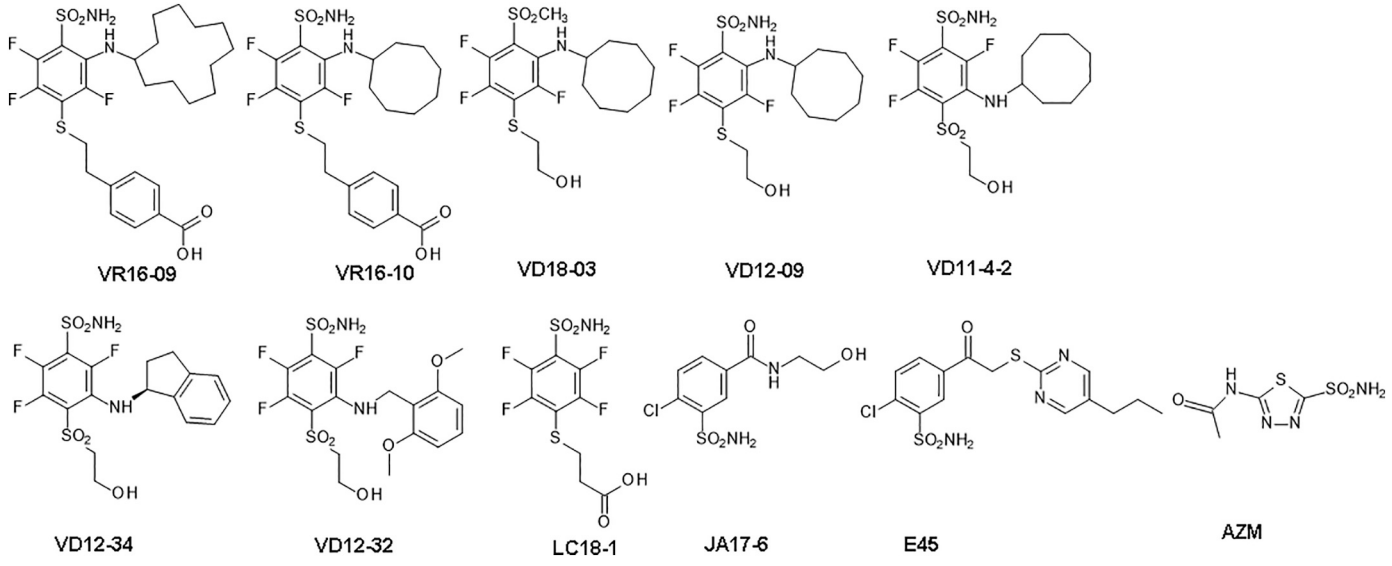

Fig. 1. Chemical structure of compounds used for this study.

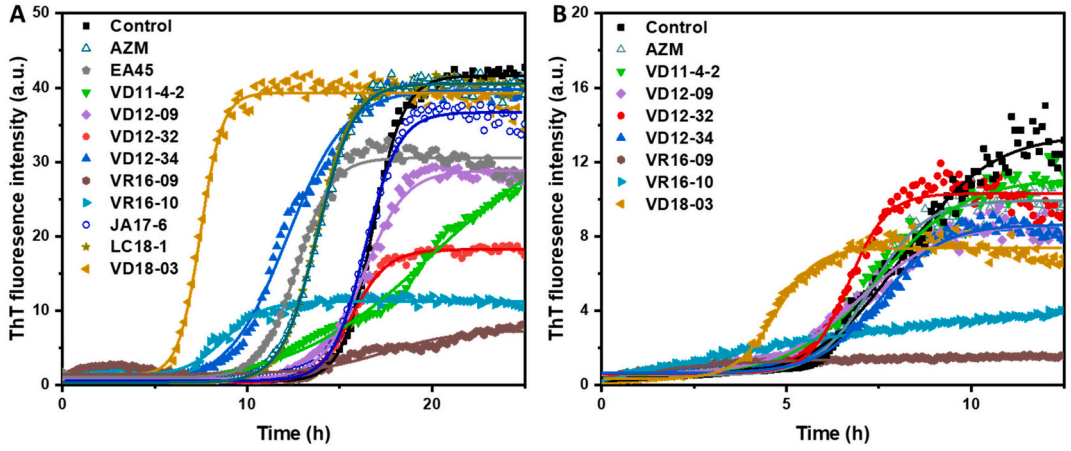

Fig. 2. The effect of 200 μM of compounds on fibrillation of A) 70 μM α-Syn and B) 50 μM Aβ fibrillation measured by ThT fluorescence.

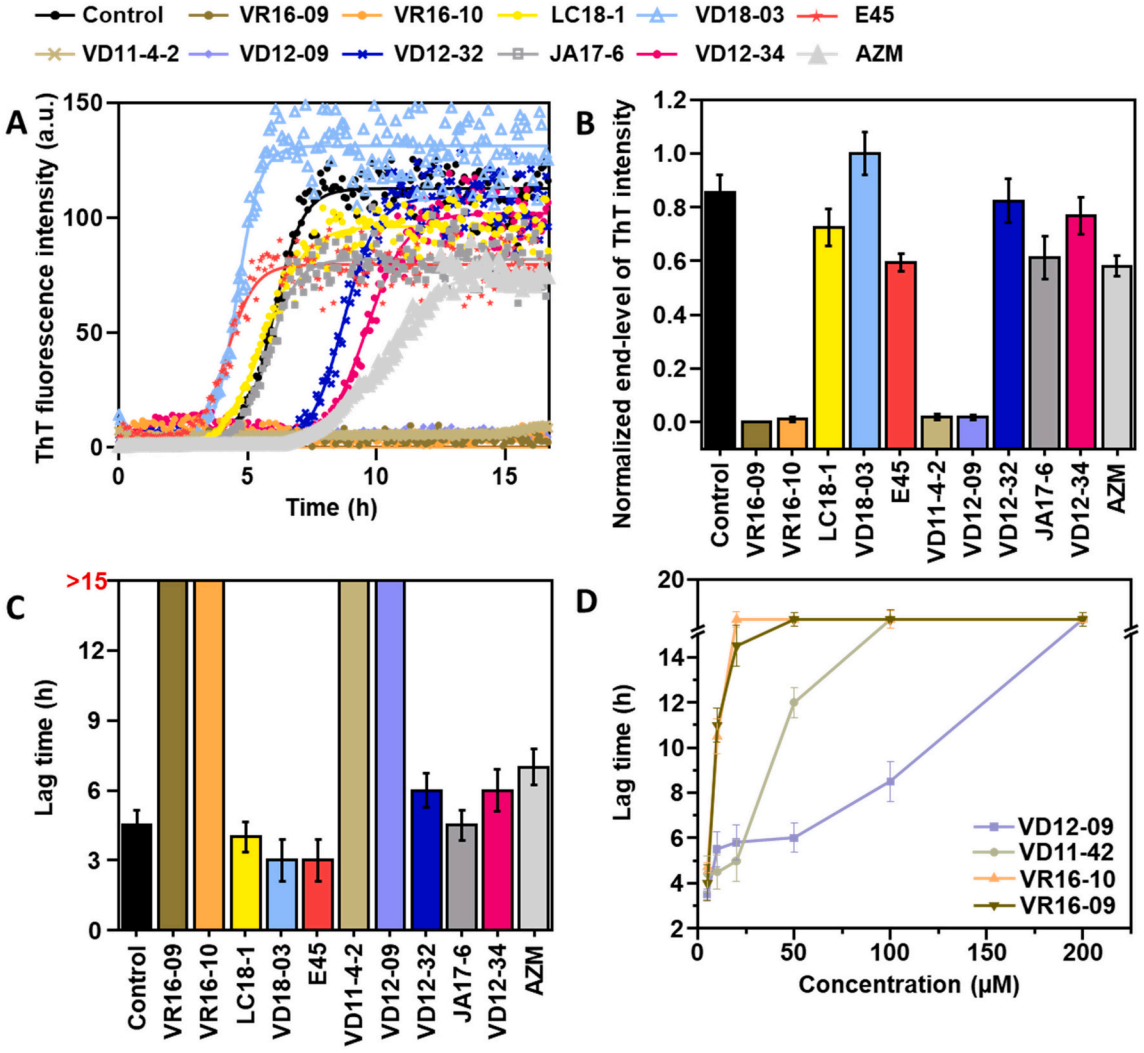

Fig. 3. The effects of 200 μM of compounds on the A) ThT fluorescence time profile, B) end level ThT fluorescence and C) lag time of insulin fibrillation obtained from ThT time curves. The columns that contain lag time values >15 h indicate no fibrillation. D) The effect of different concentration of best compounds on the lag phase of insulin fibrillation.

retained overall. Only VR16-09 completely retained the native state of insulin throughout the whole incubation period.

Chromatograms of SEC from different times of fibrillation in the absence and presence of VR16-09 and VR16-10 are provided in Fig. S3C. In the absence of compounds, the monomeric state of insulin completely disappears at the beginning of elongation phase and large oligomers are

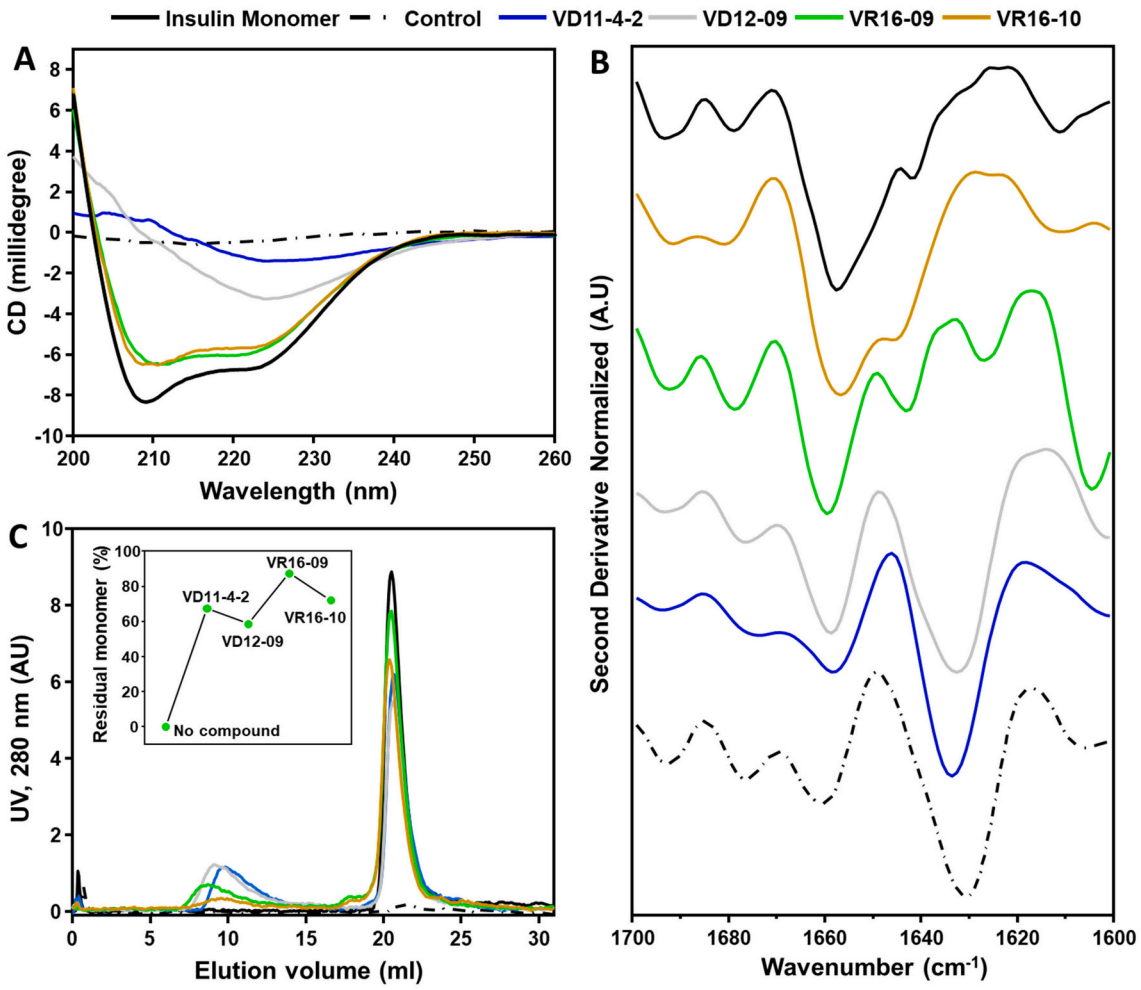

Fig. 4. Different compounds maintain insulin in the native and monomeric state to different extents as judged by A) CD spectra, B) FTIR spectra and C) SEC profiles of samples from the end point of insulin fibrillation.

formed in this phase. VR16-10 retains insulin to a greater extent in the monomeric state at all time points though with detectable levels of higher-order species. VR16-09 essentially maintains insulin completely in the monomeric state over the entire measurement period.

Thus spectroscopic and chromatographic analyses confirm the initial conclusion from ThT assays that these compounds are able to inhibit insulin aggregation.

3.3. Presence of VR16-09 and VR16-10 compounds under fibrillation condition leads to the formation of aggregates with the lowest cytotoxicity

To investigate whether fibrillation inhibition could rescue cells against aggregate toxicity, we turned to a cell viability (MTT) assay and an LDH assay. Insulin incubated alone or in the presence of VD11-4-2, VD12-09, VR16-09, and VR16-10 were incubated with human neuroblastoma SH-SY5Y cells. All four compounds increased cell viability compared to compound-free insulin aggregates. The highest cell viability was conferred by VR16-09 and VR16-10 (Fig. 5A), both of which also reduced the release of LDH compared to control (Fig. 5B).

3.4. TEM and AFM images confirmed the inhibitory effects of VR16-09 and VR16-10 compounds on insulin fibril formation

Insulin fibrils formed in the absence of any compound showed extensive fibril morphology by electron microscopy (Fig. 5C). TEM results showed that both VR16-09 and VR16-10 led to the formation of amorphous aggregates and strongly reduced the occurrence of fibrillar networks. AFM was employed to further explore the morphology of individual fibrillar structures at higher resolution (Fig. S4). We focused on samples obtained after the insulin aggregation experiment (*i.e.* when the ThT fluorescence plateau was reached) to understand the impact of the inhibitors on insulin fibril formation. The control sample (Fig. S4A) reveals fibrils up to several μm in length with an average height of 2–5 nm. The insulin sample with VR16-09 (Fig. S4B) was dominated by very small and granular structures (with rare instances of l small "lumps" up to 50 nm in height), suggesting that the VR16-09 changed the aggregation pathway from fibrils to oligomeric structures. The effect of VR16-10 is even more dramatic (Fig. S4C): there are almost no fibrillar and oligomeric species on the mica.

We next queried whether the aggregation inhibitory effects of VR16-09, VR16-10, VD11-4-2 and VD12-09 against insulin were correlated with their ability to inhibit CA activity. For this purpose the K_D of compounds against 12 recombinant human CA isozymes were obtained from previous work using thermal shift assays (Supplementary Table S1) while the lag time of insulin aggregation (derived from Fig. 3D) was used to obtain IC_{50} of inhibition. All four compounds were highly selective and low nanomolar inhibitors of CA IX isozyme, an anticancer drug target. VD11-4-2 exhibited the lowest dissociation constant (K_D = 32 pM) for CA IX, whereas its effectiveness to inhibit insulin fibril formation was lower than VR16-09 and VR16-10. Thus, there was no significant correlation between compound binding affinity for CA IX isozyme and insulin aggregation inhibition (Fig. S5). This indicates that the

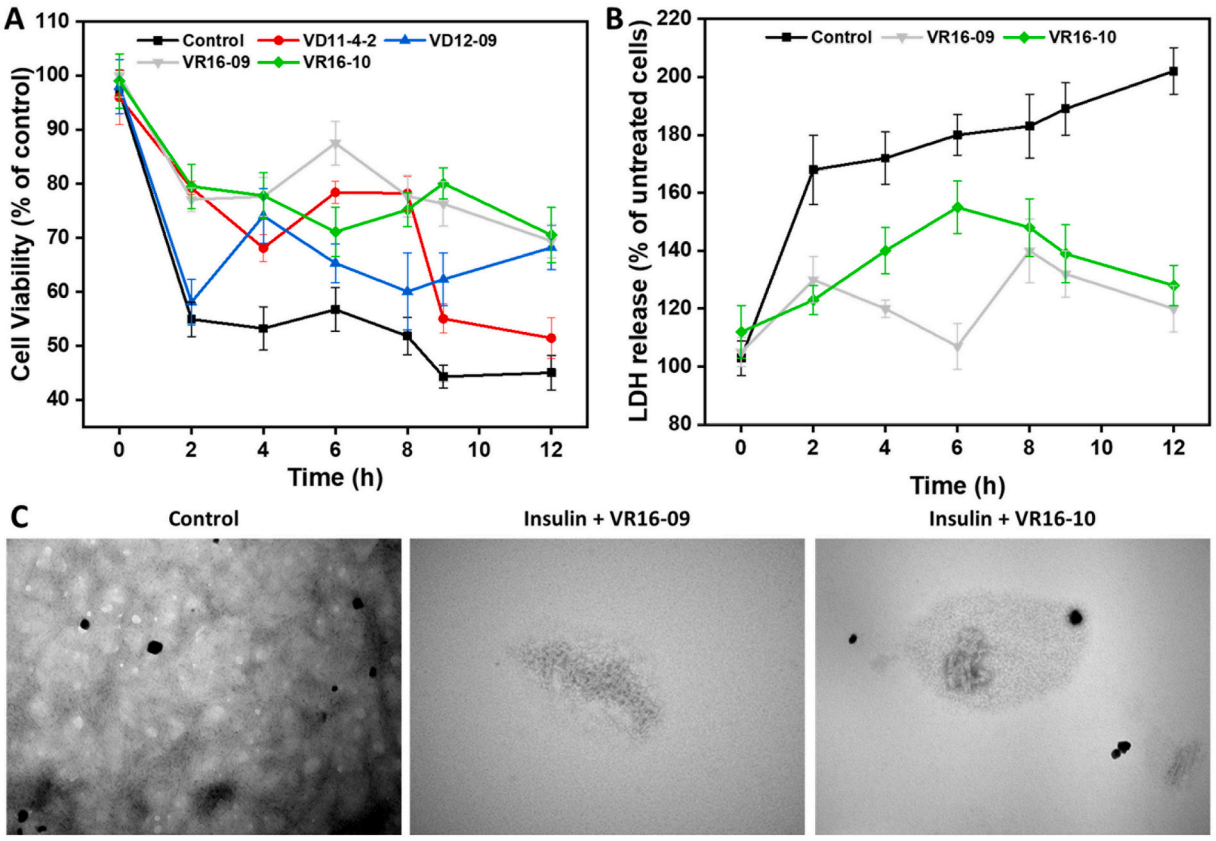

Fig. 5. Different VR compounds protect SH-SY5Y cells against insulin aggregate toxicity and maintain them in a less aggregated state. A) Cell viability and B) LDH assay of samples collected at different time of insulin fibril formation. C) TEM morphological analysis of insulin incubated in the absence and the presence of 200 μM of VR16-09 and VR16-10. Samples were collected and analyzed at the end of the fibrillation process.

inhibitory mechanism of insulin fibrillation is completely different from the mechanism of inhibition of CA activity by these compounds.

3.5. Molecular dynamics simulations of compounds interacting with insulin

We finally turned to molecular dynamics simulations to determine the interaction between insulin and both strong and weak anti-fibrillation agents. Since our experimental data had identified VR16-09 and VR16-10 as the best fibrillation inhibitors, we decided to use these two compounds in the simulations. As negative controls we used VD18-03 and VD12-34 which are poor anti-fibrillation agents but show high structural similarity to VR16-09 and VR16-10. Each ligand was randomly oriented and located around an insulin monomer, and each insulin/ligand system was simulated for 100 ns in ten separate runs, hereby ensuring that the observed collisions are not biased by the starting configuration. The root-mean-square deviation (RMSD) and fluctuation (RMSF) was calculated for each run in order to assess the stability of insulin during the simulations. From the RMSD analysis it was observed that insulin stabilizes within the first 1–2 ns in almost all repeats (Fig. S6). Only a few repeat simulations show more dynamic behavior when one of the strong anti-fibrillation ligands are nearby. The RMSF analysis revealed that the C-terminal segment of chain B was considerably more dynamic than the rest of insulin (Fig. S7).

Following confirmation of insulin stability during the simulations, the minimal distance between each ligand and insulin was determined (Fig. S8). Binding of the best anti-fibrillating agents, VR16-09 and VR16-10, to insulin was observed within 100 ns in all repeats, and no unbinding events were observed. In the case of VD18-03, a weak anti-fibrillating agent, binding was similarly observed in all ten repeats; however several unbinding events also occurred. The other weak anti-fibrillating agent, VD12-34, was only observed to bind to insulin in eight out of ten repeats and unbinding was also observed multiple times. Based on visual observations from all setups and repeats, five common interaction sites (sites A–E) between ligand and insulin were determined and shown in Fig. 6. Site A is located on top of chain A of insulin, site B is located between the helical segment in chain B and the C-terminal segment of chain B, site C is located between the helical segment in chain B and the N-terminal segment of chain B, site D is located at the N-terminal end of the helical segment of chain B and finally, site E is located at the C-terminal end of the helical segment of chain B. Binding to site D, and to some extent also site E, is often followed by the ligand moving to either site A, B or C, and site D and E are therefore considered anchor points rather than stable sites of interaction. As site D holds more polar residues than the other sites, it is a clear-cut first interaction point between ligand and insulin. Importantly, binding to site B has previously been proposed to prevent oligomerization of insulin due to disruption of the dimer interface [39].

The residence time of each ligand at each site was calculated and is reported in Fig. S9. An average residence time was not calculated due to limited observation of ligand unbinding events. The best anti-fibrillation agent, VR16-09, initially interacted with site D before moving to site B in four of the repeat simulations, while in three additional repeats the ligand remained at site D during the remainder of the 100 ns. In one repeat the ligand binds to and stays in site A for the remainder of the trajectory, and another repeat displayed similar behavior but for site C. The last simulation repeat shows the ligand initially binding to site D before moving down to site C briefly and finally ending up in site A for the remainder of the trajectory. Collectively it appears that VR16-09 prefers binding at site B, but is able to interact with insulin at other sites too. Interestingly, visual inspection showed VR16-09 to be able to wedge in between the helical and C-terminal segments of chain B

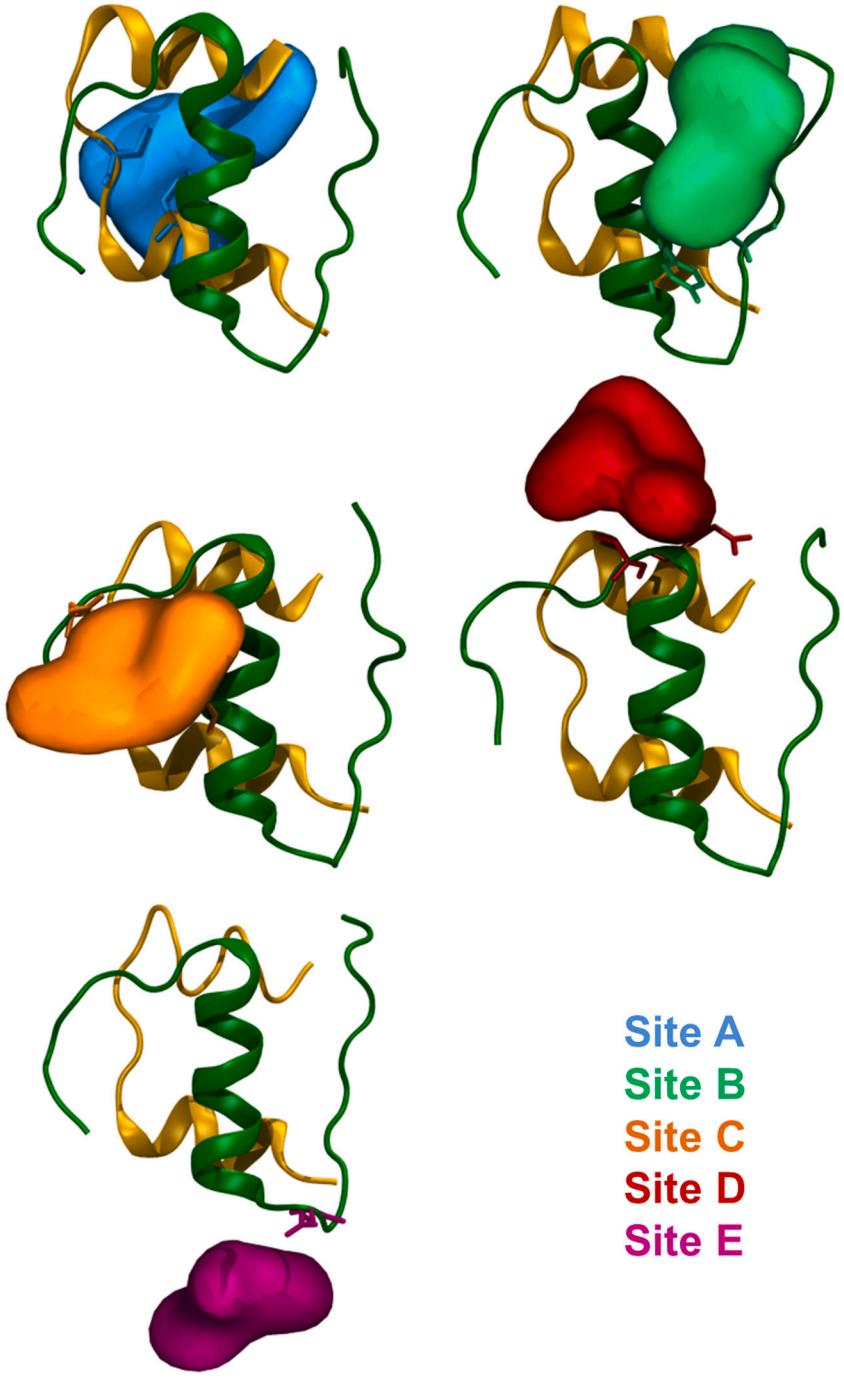

Fig. 6. Molecular dynamics simulations identify common sites of VR compound interactions with insulin as observed across all simulation setups and repeats. Site A (blue) is located on top of chain A; site B (green) between the helical segment in chain B and the C-terminal segment of chain B; site C (orange) between the helical segment in chain B and the N-terminal segment of chain B; site D (red) at the N-terminal end of the helical segment of chain B; and site E (magenta) at the C-terminal end of the helical segment of chain B. Chain A of insulin is shown as yellow ribbons, while chain B is shown in green. The residues used to define each site in the residence time calculations are shown in the same colors as each site. The volume representing each site is only indicative as it is based on a representative frame and not the trajectory as a whole. (For color references, the reader is referred to the web version of this article.)

whereby further disrupting the proposed oligomerization interface (Fig. 7). When bound to site B, the 12-membered ring of VR16-09 was often found to interact with hydrophobic residues such as $Phe24_B$, $Ile15_B$, $Val12_B$, and $Leu11_B$, while the carboxyl group often shared a hydrogen bond with $Tyr26_B$ or the N-terminus of chain A, a salt bridge with $Lys29_B$, or hydrophobic interactions with $Phe24_B$. π/π stacking of either phenyl to $Tyr29_B$ as well as polar interactions between the sulfonamide and the N-terminus of chain A was also often observed. The above observations can be condensed into the following: site B on insulin has a hydrophobic hotspot on the C-terminus-facing side of chain B's helix, a polar hotspot at the N-terminus of chain A and another polar hotspot at the C-terminal end of chain B. VR16-09 interacts with all three by placing the 12-membered ring in the hydrophobic hotspot and the sulfonamide or carboxy group interchangeably in either polar hotspot. It should be noted that these three hotspots are only accessible simultaneously because VR16-09 wedges in between the helix and C-terminal segment of chain B.

VR16-10, the second best fibrillation inhibitor, shows less preference toward site B over site A and to some extent also C. In four separate runs, VR16-10 binds to site B and stays for the remainder of the trajectory; however, as the ligand is slower to bind to insulin the resulting residence times are shorter than those observed for VR16-09. Also, in two of these repeats the initial interaction was *via* site D. In three repeats the ligand binds directly to site A and stays for the remainder of the trajectory, and in two other repeats the same was observed for site C. The last repeat shows binding to site B followed by binding to site A. Thus, consistently with the *in vitro* profile, VR16-10 preferably binds to site A and B. Additionally, when bound to site B, wedging between the helical and C-

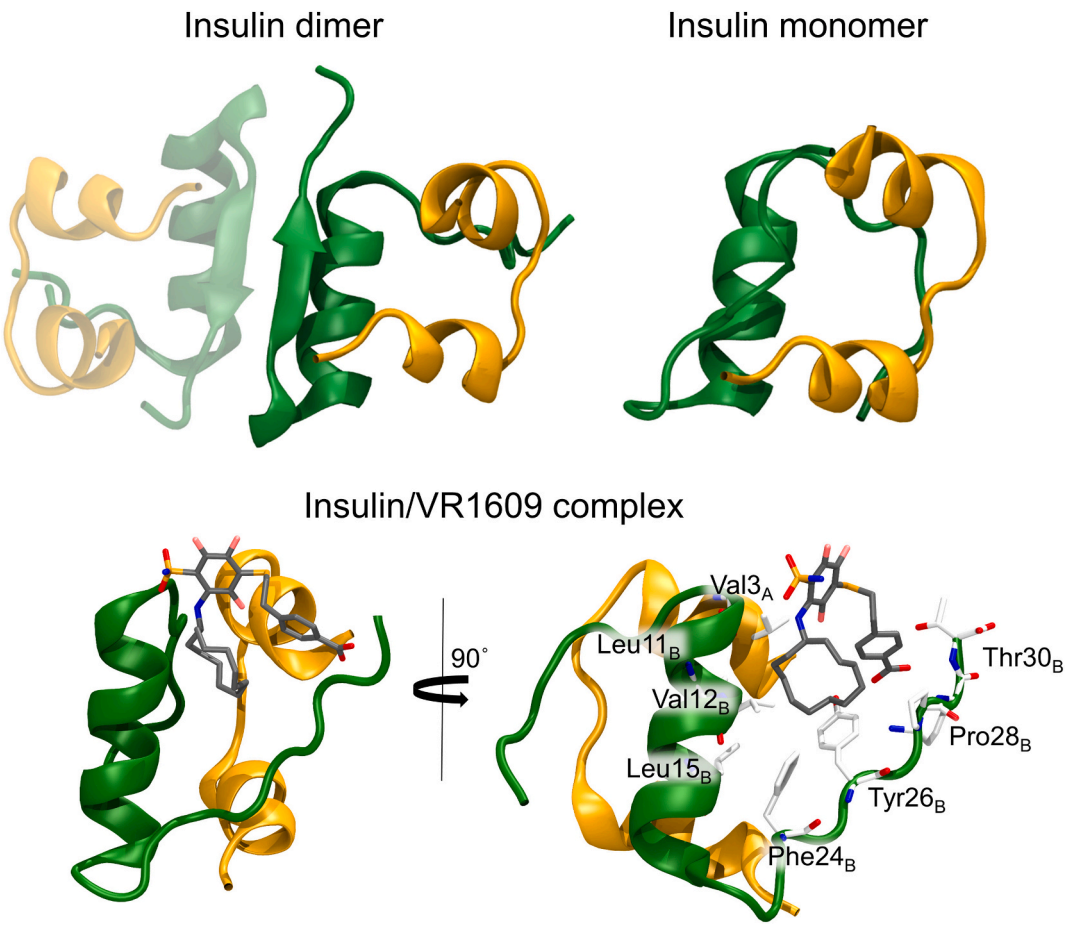

Fig. 7. VR16-09 interruption of insulin dimer formation. Insulin's dimer and monomeric states are shown as is the monomeric form bound to VR16-09 in site B. A rotated view of the complex is also shown with insulin residues within 3 Å of the ligand. Insulin's chain A is shown as yellow ribbons, while chain B is shown in green. VR16-09 is shown in gray, and protein residues are shown in white. (For color references, the reader is referred to the web version of this article.)

terminal segments of chain B was only observed once in the simulations. Simultaneous binding to the three hotspots outlined above therefore does not occur for VR16-10. The 8-membered ring was observed to interact with the hydrophobic hotspot while the polar hotspot in the C-terminal segment of chain B interacts with either sulfonamide or carboxyl group; however, more often an alternative binding mode in which two out of the three ring structures line the helical segment of chain B, while the remaining ring structure does not interact with insulin was observed.

Binding of the poor anti-fibrillating agent VD18-03 is characterized by many short-lived binding and unbinding events in each simulation repeat. Binding to site A is most common, followed by site B and then C. VD18-03 binding often initially occurred *via* site D or E before moving to one of the other sites. When VD18-03 was found in site B, it mainly interacted with the hydrophobic hotspot on the helix of chain B, or the aromatic residues in the C-terminal segment of chain B, while the remainder of the ligand rarely interacted with insulin. Similarly, VD12-34 was observed to bind and rebind multiple times in each repeat, but displays very little preference to any of the sites, although a few residence times above 50 ns were observed at sites A and B. The same interaction profile as VD18-03 was observed for VD12-34.

To summarize, VR16-09 displayed preferential binding to site B with residence times beyond our simulation timescale. VR16-10 displayed preferential binding to site A and B and similarly displayed residence times beyond our simulation setup in accord with their *in vitro* ability to prevent oligomerization and fibrillation. VD18-03 displayed considerably shorter residence times and preferred binding to sites A and B, while VD12-34 also had short residence times and displayed little to no preference between sites A, B, and C. Both observations are in accord with their poor *in vitro* anti-fibrillation ability. Thus MD simulations support our experimental data and provide direct structural insight into the interactions that drive productive binding of the fibrillation inhibitors.

4. Discussion

The fibrillation of proteins is a multi-step process, consisting of nucleation, growth, and saturation steps [56]. This study aimed to investigate the inhibitory effects of some CA inhibitors against protein fibrillation. Our work was inspired by the compounds' similarity to known inhibitors of α-Syn aggregation. Initially, we tested these compounds against α-Syn and Aβ(1-40). Given the relatively poor performance of the compounds against the fibrillation of these two intrinsically disordered proteins, we turned to the fibrillation of the native protein insulin and fortuitously discovered a much stronger effect here. The ThT assay indicated that 20–50 μM VR16-09 and VR16-10 compounds completely suppressed insulin fibrillation within the experimental time window. This observation suggests that these compounds disturbed the formation of nuclei in the lag phase of fibril formation. Samples from different stages of the fibrillation process and structural studies by CD and FTIR spectroscopy showed that VR16-09 and VR16-10 suppress structural changes of the native insulin and diminish the formation of ThT positive species. This might occur by preventing hydrophobic interactions as one of the major driving forces of amyloid aggregation. Maintaining the native state of insulin explains the ability of these compounds to reduce cytotoxicity of insulin

incubated under otherwise aggregation-promoting conditions.

Mechanistically, our MD simulations indicated that the VR16-09 compound preferentially binds around the C terminus of the B chain. A 100 ns simulation run in ten repeats showed that VR16-09 has the longest residence time in each site and the highest number of binding events among all ligands. Remarkably, VR16-09 particularly associates with $Phe24_B$ and to some extent also $Tyr16_B$ which are key residues in insulin dimerization (Fig. 7). VR16-09 and VR16-10 are the two best fibrillation inhibitors and have a similar backbone structure. However, VR16-09 has a slightly longer hydrophobic tail (an aminocyclododecyl group) than VR16-10 (an aminocyclooctyl group), indicating an enhanced binding affinity to hydrophobic residues on insulin [57]. The MD simulations revealed VR16-09 to be able to perturb insulin's conformation by wedging in between the helix and the C-terminal segment of chain B due to interaction with three hotspots of insulin (Fig. 7). VR16-10 was observed to interact with two out of the three hotspots only. Additionally, either ring structure would interact with the hydrophobic hotspot on the helical segment of chain B, while for VR16-09 it was always the 12-membered ring. This may explain the superior ability of VR16-09 to inhibit protein fibrillation compared to VR16-10. Akbarian et al. compared the inhibitory effects of different compounds against insulin fibrillation [58]. Like the compounds reported in that study, both VR16-09 and VR16-10 interact with Tyr^{B16} which is a key residue in insulin dimerization, and this interaction likely blocks insulin fibrillation sterically. Some compounds in [58] lead to formation of very small aggregates or short fibrils, but our AFM results indicate that VR16-10 largely suppresses formation of fibrils or other large aggregates.

5. Conclusion

In this study, the ability of a series of sulfonamide compounds to inhibit fibril formation was investigated. Our results showed that fluorinated sulfonamide compounds have prominent effects on insulin fibril formation and a moderate effect on α-Syn and Aβ fibril formation. The two best compounds maintained insulin in the native and monomeric state during the experimental time window with lower cell toxicity than the control sample. These results indicated that some fluorinated sulfonamide compounds have diverse therapeutic potential as inhibitors of carbonic anhydrase activity (with corresponding potential for anti-cancer effects [25–27]) as well as anti-fibrillation effects.

Author statement

The authors declare that there were no studies in humans and animals.

Declaration of competing interest

None declared.

Data availability

Data will be made available on request.

Acknowledgements

D.E.O. and B.S. thank the Lundbeck Foundation for support for work against Parkinson's disease (grant R276-2018-671). D.M. and V.D. thank the Research Council of Lithuania (grant 01.2.2-LMT-K-718-03-0003). All computations were made possible at the Grendel cluster through the Centre for Scientific Computing, Aarhus (http://www.cscaa.dk/grendel/hardware/).

Appendix A. Supplementary data

Supplementary data to this article can be found online at https://doi.org/10.1016/j.ijbiomac.2022.12.105.

References

[1] J.W. Kelly, The alternative conformations of amyloidogenic proteins and their multi-step assembly pathways, Curr. Opin. Struct. Biol. 8 (1998) 101–106, https://doi.org/10.1016/S0959-440X(98)80016-X.
[2] M. Fändrich, M.A. Fletcher, C.M. Dobson, Amyloid fibrils from muscle myoglobin, Nature 410 (2001) 165–166, https://doi.org/10.1038/35065514.
[3] K. Morris, L. Serpell, From natural to designer self-assembling biopolymers, the structural characterisation of fibrous proteins & peptides using fibre diffraction, Chem. Soc. Rev. 39 (2010) 3445, https://doi.org/10.1039/b919453n.
[4] D.J. Selkoe, Folding proteins in fatal ways, Nature 426 (2003) 900–904, https://doi.org/10.1038/nature02264.
[5] V. Uversky, The triple power of D3: protein intrinsic disorder in degenerative diseases, Front. Biosci. 19 (2014) 181, https://doi.org/10.2741/4204.
[6] M. Jucker, L.C. Walker, Self-propagation of pathogenic protein aggregates in neurodegenerative diseases, Nature 501 (2013) 45–51, https://doi.org/10.1038/nature12481.
[7] F. Chiti, C.M. Dobson, Protein misfolding, functional amyloid, and human disease, Annu. Rev. Biochem. 75 (2006) 333–366, https://doi.org/10.1146/annurev.biochem.75.101304.123901.
[8] J. Götz, L.M. Ittner, Y.-A. Lim, Common features between diabetes mellitus and Alzheimer's disease, Cell. Mol. Life Sci. 66 (2009) 1321–1325, https://doi.org/10.1007/s00018-009-9070-1.
[9] C.M. Dobson, Protein folding and misfolding, Nature 426 (2003) 884–890, https://doi.org/10.1038/nature02261.
[10] J. Hardy, The amyloid hypothesis of Alzheimer's disease: progress and problems on the road to therapeutics, Science (80-.) 297 (2002) 353–356, https://doi.org/10.1126/science.1072994.
[11] S.L. Bernstein, N.F. Dupuis, N.D. Lazo, T. Wyttenbach, M.M. Condron, G. Bitan, D. B. Teplow, J.-E. Shea, B.T. Ruotolo, C.V. Robinson, M.T. Bowers, Amyloid-β protein oligomerization and the importance of tetramers and dodecamers in the aetiology of Alzheimer's disease, Nat. Chem. 1 (2009) 326–331, https://doi.org/10.1038/nchem.247.
[12] V.N. Uversky, A.L. Fink, Conformational constraints for amyloid fibrillation: the importance of being unfolded, Biochim. Biophys. Acta, Proteins Proteomics 1698 (2004) 131–153, https://doi.org/10.1016/j.bbapap.2003.12.008.
[13] M. Biancalana, S. Koide, Molecular mechanism of thioflavin-T binding to amyloid fibrils, Biochim. Biophys. Acta, Proteins Proteomics 2010 (1804) 1405–1412, https://doi.org/10.1016/j.bbapap.2010.04.001.
[14] D.E. Otzen, Amyloid Fibrils and Prefibrillar Aggregates, Wiley-VCH Verlag GmbH & Co. KGaA, Weinheim, Germany, 2013, https://doi.org/10.1002/9783527654185.
[15] C.G. Glabe, Common mechanisms of amyloid oligomer pathogenesis in degenerative disease, Neurobiol. Aging 27 (2006) 570–575, https://doi.org/10.1016/j.neurobiolaging.2005.04.017.
[16] T.S. Jarvela, H.A. Lam, M. Helwig, N. Lorenzen, D.E. Otzen, P.J. McLean, N. T. Maidment, I. Lindberg, The neural chaperone proSAAS blocks α-synuclein fibrillation and neurotoxicity, Proc. Natl. Acad. Sci. 113 (2016) E4708–E4715, https://doi.org/10.1073/pnas.1601091113.
[17] H. Mohammad-Beigi, F. Aliakbari, C. Sahin, C. Lomax, A. Tawfike, N.P. Schafer, A. Amiri-Nowdijeh, H. Eskandari, I.M. Møller, M. Hosseini-Mazinani, G. Christiansen, J.L. Ward, D. Morshedi, D.E. Otzen, Oleuropein derivatives from olive fruit extracts reduce α-synuclein fibrillation and oligomer toxicity, J. Biol. Chem. 294 (2019) 4215–4232, https://doi.org/10.1074/jbc.RA118.005723.
[18] H. Mohammad-Beigi, A. Hosseini, M. Adeli, M.R. Ejtehadi, G. Christiansen, C. Sahin, Z. Tu, M. Tavakol, A. Dilmaghani-Marand, I. Nabipour, F. Farzadfar, D. E. Otzen, M. Mahmoudi, M.J. Hajipour, Mechanistic understanding of the interactions between Nano-objects with different surface properties and α-synuclein, ACS Nano 13 (2019) 3243–3256, https://doi.org/10.1021/acsnano.8b08983.
[19] K.M. Pate, B.J. Kim, E.V. Shusta, R.M. Murphy, Transthyretin mimetics as anti-β-amyloid agents: a comparison of peptide and protein approaches, ChemMedChem 13 (2018) 968–979, https://doi.org/10.1002/cmdc.201800031.
[20] V. Sharma, K.S. Ghosh, Inhibition of amyloid fibrillation by small molecules and nanomaterials: strategic development of pharmaceuticals against amyloidosis, Protein Pept. Lett. 26 (2019) 315–323, https://doi.org/10.2174/0929866526666190307164944.
[21] T.I. Chandel, N. Zaidi, M. Zaman, I. Jahan, A. Masroor, I.A. Siddique, S.M. Nayeem, M. Ali, V.N. Uversky, R.H. Khan, A multiparametric analysis of the synergistic impact of anti-Parkinson's drugs on the fibrillation of human serum albumin, Biochim. Biophys. Acta, Proteins Proteomics 2019 (1867) 275–285, https://doi.org/10.1016/j.bbapap.2018.10.003.
[22] H. Sun, J. Liu, S. Li, L. Zhou, J. Wang, L. Liu, F. Lv, Q. Gu, B. Hu, Y. Ma, S. Wang, Reactive amphiphilic conjugated polymers for inhibiting amyloid β assembly, Angew. Chem. 131 (2019) 6049–6054, https://doi.org/10.1002/ange.201901459.
[23] M. Kurnik, C. Sahin, C.B. Andersen, N. Lorenzen, L. Giehm, H. Mohammad-Beigi, C.M. Jessen, J.S. Pedersen, G. Christiansen, S.V. Petersen, R. Staal, G. Krishnamurthy, K. Pitts, P.H. Reinhart, F.A.A. Mulder, S. Mente, W.D. Hirst, D. E. Otzen, Potent α-synuclein aggregation inhibitors, identified by high-throughput screening, mainly target the monomeric state, Cell Chem. Biol. 25 (2018) 1389–1402, https://doi.org/10.1016/j.chembiol.2018.08.005, e9.

[24] R.G. Khalifah, Carbon dioxide hydration activity of carbonic anhydrase: paradoxical consequences of the unusually rapid catalysis, Proc. Natl. Acad. Sci. 70 (1973) 1986–1989, https://doi.org/10.1073/pnas.70.7.1986.
[25] B.-B. Gao, A. Clermont, S. Rook, S.J. Fonda, V.J. Srinivasan, M. Wojtkowski, J. G. Fujimoto, R.L. Avery, P.G. Arrigg, S.-E. Bursell, L.P. Aiello, E.P. Feener, Extracellular carbonic anhydrase mediates hemorrhagic retinal and cerebral vascular permeability through prekallikrein activation, Nat. Med. 13 (2007) 181–188, https://doi.org/10.1038/nm1534.
[26] N. Hen, M. Bialer, B. Yagen, A. Maresca, M. Aggarwal, A.H. Robbins, R. McKenna, A. Scozzafava, C.T. Supuran, Anticonvulsant 4-aminobenzenesulfonamide derivatives with branched-alkylamide moieties: X-ray crystallography and inhibition studies of human carbonic anhydrase isoforms I, II, VII, and XIV, J. Med. Chem. 54 (2011) 3977–3981, https://doi.org/10.1021/jm200209n.
[27] O. Guler, G. Simone, C. Supuran, Drug design studies of the novel antitumor targets carbonic anhydrase IX and XII, Curr. Med. Chem. 17 (2010) 1516–1526, https://doi.org/10.2174/092986710790979999.
[28] V.M. Krishnamurthy, G.K. Kaufman, A.R. Urbach, I. Gitlin, K.L. Gudiksen, D. B. Weibel, G.M. Whitesides, Carbonic anhydrase as a model for biophysical and physical-organic studies of proteins and Protein−Ligand binding, Chem. Rev. 108 (2008) 946–1051, https://doi.org/10.1021/cr050262p.
[29] V.M. Krishnamurthy, G.K. Kaufman, A.R. Urbach, I. Gitlin, K.L. Gudiksen, D. B. Weibel, G.M. Whitesides, Carbonic anhydrase as a model for biophysical and physical-organic studies of proteins and Protein−Ligand binding, Chem. Rev. 108 (2008) 946–1051, https://doi.org/10.1021/cr050262p.
[30] V. Linkuvienė, A. Zubrienė, E. Manakova, V. Petrauskas, L. Baranauskienė, A. Zakšauskas, A. Smirnov, S. Gražulis, J.E. Ladbury, D. Matulis, Thermodynamic, kinetic, and structural parameterization of human carbonic anhydrase interactions toward enhanced inhibitor design, Q. Rev. Biophys. 51 (2018), e10, https://doi.org/10.1017/S0033583518000082.
[31] G. Chen, T. Xu, Y. Yan, Y. Zhou, Y. Jiang, K. Melcher, H.E. Xu, Amyloid beta: structure, biology and structure-based therapeutic development, Acta Pharmacol. Sin. 38 (2017) 1205–1235, https://doi.org/10.1038/aps.2017.28.
[32] B. Swift, Examination of insulin injection sites: an unexpected finding of localized amyloidosis, Diabet. Med. 19 (2002) 881–882, https://doi.org/10.1046/j.1464-5491.2002.07581.x.
[33] F.E. Dische, C. Wernstedt, G.T. Westermark, P. Westermark, M.B. Pepys, J. A. Rennie, S.G. Gilbey, P.J. Watkins, Insulin as an amyloid-fibril protein at sites of repeated insulin injections in a diabetic patient, Diabetologia 31 (1988) 158–161, https://doi.org/10.1007/BF00276849.
[34] J. Brange, L. Langkjœr, in: Insulin Structure and Stability, 1993, pp. 315–350, https://doi.org/10.1007/978-1-4899-1236-7_11.
[35] C. Bryant, D.B. Spencer, A. Miller, D.L. Bakaysa, K.S. McCune, S.R. Maple, A. H. Pekar, D.N. Brems, Acid stabilization of insulin, Biochemistry 32 (1993) 8075–8082, https://doi.org/10.1021/bi00083a004.
[36] Y. Ohno, T. Seki, Y. Kojima, R. Miki, Y. Egawa, O. Hosoya, K. Kasono, T. Seki, Investigation of factors that cause insulin precipitation and/or amyloid formation in insulin formulations, J. Pharm. Health Care Sci. 5 (2019) 22, https://doi.org/10.1186/s40780-019-0151-5.
[37] M.R. Nilsson, Insulin amyloid at injection sites of patients with diabetes, Amyloid 23 (2016) 139–147, https://doi.org/10.1080/13506129.2016.1179183.
[38] M. Nakamura, Y. Misumi, T. Nomura, W. Oka, A. Isoguchi, K. Kanenawa, T. Masuda, T. Yamashita, Y. Inoue, Y. Ando, M. Ueda, Extreme adhesion activity of amyloid fibrils induces subcutaneous insulin resistance, Diabetes 68 (2019) 609–616, https://doi.org/10.2337/db18-0846.
[39] S.H. Alijanvand, M.H. Christensen, G. Christiansen, K.B. Harikandei, P. Salehi, B. Schiøtt, A.A. Moosavi-Movahedi, D.E. Otzen, Novel noscapine derivatives stabilize the native state of insulin against fibrillation, Int. J. Biol. Macromol. 147 (2020) 98–108, https://doi.org/10.1016/j.ijbiomac.2020.01.061.
[40] F. Longhena, G. Faustini, V. Brembati, M. Pizzi, A. Bellucci, The good and bad of therapeutic strategies that directly target α-synuclein, IUBMB Life 72 (2020) 590–600, https://doi.org/10.1002/iub.2194.
[41] N. Lorenzen, S.B. Nielsen, A.K. Buell, J.D. Kaspersen, P. Arosio, B.S. Vad, W. Paslawski, G. Christiansen, Z. Valnickova-Hansen, M. Andreasen, J.J. Enghild, J.S. Pedersen, C.M. Dobson, T.P.J. Knowles, D.E. Otzen, The role of stable α-synuclein oligomers in the molecular events underlying amyloid formation, J. Am. Chem. Soc. 136 (2014) 3859–3868, https://doi.org/10.1021/ja411577t.
[42] D. Baronas, V. Dudutienė, V. Paketurytė, V. Kairys, A. Smirnov, V. Juozapaitienė, A. Vaškevičius, E. Manakova, S. Gražulis, A. Zubrienė, D. Matulis, Structure and mechanism of secondary sulfonamide binding to carbonic anhydrases, Eur. Biophys. J. 50 (2021) 993–1011, https://doi.org/10.1007/s00249-021-01561-1.
[43] V. Dudutienė, A. Zubrienė, A. Smirnov, D.D. Timm, J. Smirnovienė, J. Kazokaitė, V. Michailovienė, A. Zakšauskas, E. Manakova, S. Gražulis, D. Matulis, Functionalization of fluorinated benzenesulfonamides and their inhibitory properties toward carbonic anhydrases, ChemMedChem 10 (2015) 662–687, https://doi.org/10.1002/cmdc.201402490.
[44] S. Strazdaite, S.J. Roeters, A. Sakalauskas, T. Sneideris, J. Kirschner, K.B. Pedersen, B. Schiøtt, F. Jensen, T. Weidner, V. Smirnovas, G. Niaura, Interaction of amyloid-β-(1–42) peptide and its aggregates with Lipid/Water interfaces probed by vibrational sum-frequency generation spectroscopy, J. Phys. Chem. B 125 (2021) 11208–11218, https://doi.org/10.1021/acs.jpcb.1c04882.
[45] E. Ciszak, G.D. Smith, Crystallographic evidence for dual coordination around zinc in the T3R3 human insulin hexamer, Biochemistry 33 (1994) 1512–1517, https://doi.org/10.1021/bi00172a030.
[46] K. Vanommeslaeghe, E. Hatcher, C. Acharya, S. Kundu, S. Zhong, J. Shim, E. Darian, O. Guvench, P. Lopes, I. Vorobyov, A.D. Mackerell, CHARMM general force field: a force field for drug-like molecules compatible with the CHARMM all-atom additive biological force fields, J. Comput. Chem. (2009), https://doi.org/10.1002/jcc.21367. NA-NA.
[47] K. Vanommeslaeghe, A.D. MacKerell, Automation of the CHARMM general force field (CGenFF) I: bond perception and atom typing, J. Chem. Inf. Model. 52 (2012) 3144–3154, https://doi.org/10.1021/ci300363c.
[48] K. Vanommeslaeghe, E.P. Raman, A.D. MacKerell, Automation of the CHARMM general force field (CGenFF) II: assignment of bonded parameters and partial atomic charges, J. Chem. Inf. Model. 52 (2012) 3155–3168, https://doi.org/10.1021/ci3003649.
[49] M.J. Abraham, T. Murtola, R. Schulz, S. Páll, J.C. Smith, B. Hess, E. Lindahl, GROMACS: high performance molecular simulations through multi-level parallelism from laptops to supercomputers, SoftwareX 1–2 (2015) 19–25, https://doi.org/10.1016/j.softx.2015.06.001.
[50] J. Huang, S. Rauscher, G. Nawrocki, T. Ran, M. Feig, B.L. de Groot, H. Grubmüller, A.D. MacKerell, CHARMM36m: an improved force field for folded and intrinsically disordered proteins, Nat. Methods 14 (2017) 71–73, https://doi.org/10.1038/nmeth.4067.
[51] S.R. Durell, B.R. Brooks, A. Ben-Naim, Solvent-induced forces between two hydrophilic groups, J. Phys. Chem. 98 (1994) 2198–2202, https://doi.org/10.1021/j100059a038.
[52] W. Yu, X. He, K. Vanommeslaeghe, A.D. MacKerell, Extension of the CHARMM general force field to sulfonyl-containing compounds and its utility in biomolecular simulations, J. Comput. Chem. 33 (2012) 2451–2468, https://doi.org/10.1002/jcc.23067.
[53] I. Soteras Gutiérrez, F.-Y. Lin, K. Vanommeslaeghe, J.A. Lemkul, K.A. Armacost, C. L. Brooks, A.D. MacKerell, Parametrization of halogen bonds in the CHARMM general force field: improved treatment of ligand–protein interactions, Bioorg. Med. Chem. 24 (2016) 4812–4825, https://doi.org/10.1016/j.bmc.2016.06.034.
[54] B. Hess, P-LINCS: a parallel linear constraint solver for molecular simulation, J. Chem. Theory Comput. 4 (2008) 116–122, https://doi.org/10.1021/ct700200b.
[55] K. Gade Malmos, L.M. Blancas-Mejia, B. Weber, J. Buchner, M. Ramirez-Alvarado, H. Naiki, D. Otzen, ThT 101: a primer on the use of thioflavin T to investigate amyloid formation, Amyloid 24 (2017) 1–16, https://doi.org/10.1080/13506129.2017.1304905.
[56] A.K. Buell, The growth of amyloid fibrils: rates and mechanisms, Biochem. J. 476 (2019) 2677–2703, https://doi.org/10.1042/BCJ20160868.
[57] J. Kazokaitė, R. Niemans, V. Dudutienė, H.M. Becker, J. Leitāns, A. Zubrienė, L. Baranauskienė, G. Gondi, R. Zeidler, J. Matulienė, K. Tārs, A. Yaromina, P. Lambin, L.J. Dubois, D. Matulis, Novel fluorinated carbonic anhydrase IX inhibitors reduce hypoxia-induced acidification and clonogenic survival of cancer cells, Oncotarget 9 (2018), https://doi.org/10.18632/oncotarget.25508.
[58] M. Akbarian, R. Yousefi, F. Farjadian, V.N. Uversky, Insulin fibrillation: toward strategies for attenuating the process, Chem. Commun. 56 (2020) 11354–11373, https://doi.org/10.1039/D0CC05171C.